SAND2019-8972B

III-Nitride Ultra-Wide-Bandgap Electronic Devices

(Chapter 12 of III-Nitride Electronic Devices, edited by R. Chu)

R. J. Kaplar, A. A. Allerman, A. M. Armstrong, A. G. Baca, M. H. Crawford, J. R. Dickerson, E. A. Douglas, A. J. Fischer, B. A. Klein, and S. Reza

Sandia National Laboratories, Albuquerque, NM, USA

Abstract

This chapter discusses the motivation for the use of Ultra-Wide-Bandgap Aluminum Gallium Nitride semiconductors for power switching and radio-frequency applications. A review of the relevant figures of merit for both vertical and lateral power switching devices, as well as lateral radio-frequency devices, is presented, demonstrating the potential superior performance of these devices relative to Gallium Nitride. Additionally, representative results from the literature for each device type are reviewed, highlighting recent progress as well as areas for further research.

I. Introduction

As discussed in the previous chapters of this book, Wide-Bandgap (WBG) Gallium Nitride (GaN)-based electronic devices have resulted in dramatic improvements in applications areas such as power switching [1,2] and Radio-Frequency (RF) electronics [3,4]. As these devices become mature, researchers are now investigating the next class of semiconductor materials that may result in further improvements in device and system performance, which are known as the Ultra-Wide-Bandgap (UWBG) semiconductors [5,6]. These materials are loosely defined as those having bandgaps exceeding that of GaN (3.4 eV). Representative materials in this family are Gallium Oxide (Ga_2O_3), Diamond (C), and Aluminum Nitride / Aluminum Gallium Nitride ($AlN/Al_xGa_{1-x}N$), with others on the horizon such as cubic Boron Nitride (c-BN) and the transmission metal nitrides. The primary material property driving the development of

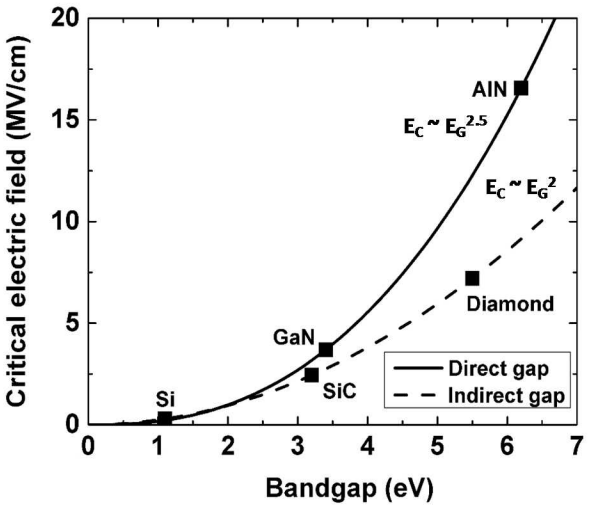

Fig. 1. Predicted critical electric field as a function of bandgap derived from Ref. [8], plotted as a function of bandgap. The points for the indicated materials are not experimental data, but rather simply indicate where each material lies on the theoretical curve.

Sandia National Laboratories is a multimission laboratory managed and operated by National Technology & Engineering Solutions of Sandia, LLC, a wholly owned subsidiary of Honeywell International Inc., for the U.S. Department of Energy's National Nuclear Security Administration under contract DE-NA0003525.

these emerging materials for electronic devices is the critical electric field, defined as the electric field at the boundary of a uniformly-doped, non-punch-through drift region (usually at a p^+-n^- or Schottky junction) that leads to avalanche breakdown [7]. Most workers in the field cite the paper by Hudgins et al. [8] that postulates a power-law relationship between the critical electric field (E_C) and the bandgap (E_G): $E_C \sim E_G^{2.0}$ for indirect-gap materials, and $E_C \sim E_G^{2.5}$ for direct-gap materials. These relationships are based on empirical fits to experimental data and oversimplify the situation somewhat (e.g. critical electric field is not constant for a given material, but rather depends on factors such as doping density and temperature) and further, the exact nature of the relationship between E_C and E_G is a topic of current theoretical and experimental inquiry. Nevertheless, it is clear that E_C increases rapidly with increasing E_G. A plot of the expected dependence of E_C on E_G, based on the equations provided in Ref. [8], is shown in Fig. 1. As will be discussed in later sections, the increasing E_C allows further improvement in the performance of UWBG devices relative to WBG devices. While all of the UWBG materials are expected to exhibit larger E_C than today's WBG materials, the AlN/AlGaN system possesses some advantages that the others do not. First, UWBG AlN/AlGaN is to a degree compatible with the mature AlGaN/GaN system (for AlGaN/GaN heterostructures the Al% is typically less than 30%, which in this case is considered to WBG rather than UWBG) and may leverage the considerable investments made in this technology over the last several decades. Further, the availability of the $Al_yGa_{1-y}N/Al_xGa_{1-x}N$ heterostructure affords a great deal of design flexibility for Al-rich AlGaN-based devices. Related to this, while impurity doping is known to be challenging for all UWBG semiconductors [5] including AlGaN (especially for holes) [9], the polarization inherent in the ternary AlGaN alloy system may be used to induce polarization doping [10], potentially supplementing or even completely circumventing the need for impurity doping.

The remainder of this chapter examines three classes of UWBG AlGaN devices: Vertical and lateral power switching devices [11], and lateral RF devices. Each section is further divided into a sub-section that describes the motivation for the use of AlGaN for that type of device, based chiefly on an analysis of the relevant Figure-of-Merit (FOM), followed by a second sub-section that provides an overview of relevant reports in the literature of each device type.

II. Vertical AlGaN Power Switching Devices

A. Motivation

The motivation for moving to higher bandgaps and critical electric fields for vertical power switching devices is most often described in terms of the Unipolar (or Baliga) FOM (UFOM). The geometry relevant to the UFOM is shown in Fig. 2. This figure depicts the electric field profile on the low-doped side of a one-dimensional junction, which is typically a p^+-n^- or Schottky junction. The thick, low-doped drift region is typically n-type due to the higher mobility of electrons

compared to holes. For a uniformly-doped drift region, the electric field profile is a linear function of position, and if the depletion region thickness (W_{Dep}) at breakdown is less than the drift region thickness (W_{Drift}), the field assumes a triangular profile, which is termed a non-punch-through case. If the drift region is fully depleted (termed punch-through) the analysis is slightly different, but the main conclusions obtained are still valid. Breakdown occurs when the field at the junction equals the critical field. For a given blocking voltage, therefore, a higher critical field permits the use of a thinner drift region, since the breakdown voltage is equal to the area under the field-position curve. This results in a lower resistance to the flow of electrons when the junction is not depleted (i.e. when the device is in the conducting on-state).

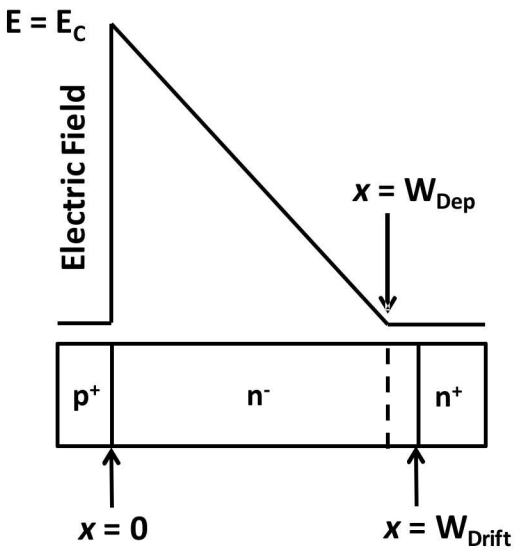

Fig. 2. Plot of electric field vs position for a one-sided, uniformly doped junction, applicable to vertical power devices characterized by the UFOM.

The trade-off between blocking voltage V_B and specific on-resistance $R_{on,sp}$ (equal to the resistance of the device when conducing, multiplied by the device area) is quantified by the UFOM:

$$UFOM = \frac{V_B^2}{R_{on,sp}} = \frac{\varepsilon \mu_n E_C^3}{4} \quad (1)$$

This expression may be derived by considering the area under the curve in Fig. 2, Gauss' law (which is where the permittivity ε in the expression originates), and the transport of electrons by drift through the depletion region. This expression does not consider bipolar transport, and bipolar devices such as Insulated-Gate Bipolar Transistors (IGBTs) can break the "limit" imposed by the UFOM. It is seen that the UFOM depends on the cube of the critical electric field, so a very large improvement in UFOM (i.e. a lower specific on-resistance for a given blocking voltage) may be expected as E_G, and hence E_C, increases. Indeed, if $E_C \sim E_G^{2.5}$ for a direct-gap material such as AlGaN as postulated above, then UFOM ~ $E_G^{7.5}$! While the UFOM is not necessarily an accurate predictor of the power density of a power converter [6], it is nevertheless a good starting point from which to evaluate the merits of a particular semiconductor for use in a vertical power device. Plots of the UFOM, expressed as $R_{on,sp}$ as a function of V_B, are shown in Fig. 3 [5]. Of course, the specific positions of the lines depend upon the material parameters that are used to calculate them, which are somewhat open to debate. The lines shown use the best-known material parameters as tabulated in Ref. [5], although it is expected that these values will be updated as more work is done on these materials. Despite this, the trend is clear, with the UWBG materials, including AlN,

moving to the lower-right of the figure, indicating lower specific on-resistance for a given breakdown voltage.

The mobility μ_n, which is the bulk electron mobility in the drift region, also appears in the UFOM. For AlGaN, this is significant because μ_n is a strong function of the alloy composition, due to alloy scattering. Various groups have performed theoretical and experimental studies of the mobility as a function of alloy composition [12,13]. The result of one such study is shown in Fig. 4. The contributions from the various scattering mechanisms considered, including alloy scattering (Alloy), polar optical phonons (OP), deformation potential (DP), piezoelectric scattering (PE), and lattice imperfections (LAT) are indicated, as well as the total mobility (green curve) as determined by Matthiessen's rule. It is apparent that the mobility is dominated by alloy scattering over nearly the entire compositional range. This has significant consequences for vertical devices fabricated from AlGaN. As the Al% in AlGaN increases from the binary GaN endpoint, E_C will increase but μ_n will decrease, and whether the UFOM experiences a net increase or decrease depends on the specific alloy composition. For low compositions, the UFOM will decrease, as E_C has not yet increased sufficiently to overcome the decrease in μ_n. However, as the Al% is further increased, the increase in E_C will overcome the lower μ_n, and a (considerable) net increase in the UFOM is achieved. This

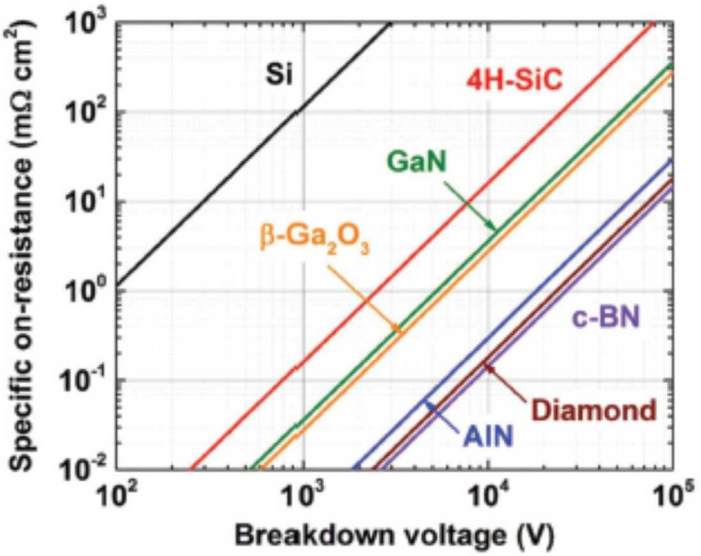

Fig. 3. Specific on-resistance plotted versus breakdown voltage based on the UFOM, Eq. (1). The lines are based on the best-known material parameters tabulated in Ref. [5]. Reprinted from Ref. [5] with permission.

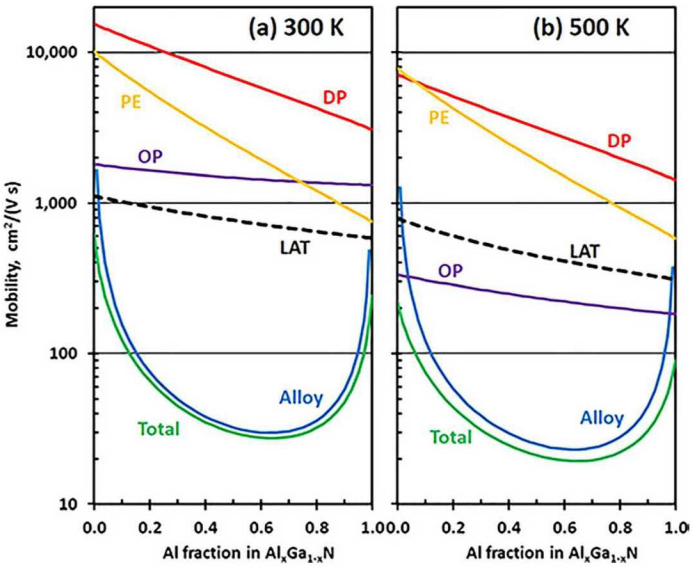

Fig. 4. Calculated bulk electron mobility in AlGaN as a function of Al fraction. Two temperatures are shown, 300 and 500 K. Reprinted from Ref. [12] with permission.

implies that higher Al% is desired for AlGaN-based devices. One other consequence of the dominance of alloy scattering in the AlGaN mobility is worthy of note, which is that the temperature dependence of alloy scattering is weak. Thus, the mobility of AlGaN will be insensitive to temperature, so while the mobility of AlGaN is lower than that of GaN, it is expected to be stable over a wide temperature range, suggesting that Al-rich AlGaN devices may be very useful for high-temperature applications. This is likely an advantage compared to GaN, where the mobility is dominated by phonon scattering, which is temperature-dependent.

B. Devices

Relatively few reports of vertical AlGaN power devices exist in the literature, and those that do exist are focused on diodes rather than transistors. Several early papers on pin diodes of varying Al compositions in AlGaN (up to 57%) were published by Nishikawa et al. [14,15]. The anode layers of these devices were composed of GaN rather than an Al composition matching that of the n-drift layer, presumably to lower the on-resistance. Further, these diodes were grown on conducting SiC substrates, permitting the fabrication of true vertical structures. Low specific on-resistance (~1.5 m$\Omega\cdot$cm^2) was thus achieved. However, very thin drift regions (~200 nm) limited the breakdown voltage, resulting in V_B < 200 V for the $Al_{0.57}Ga_{0.43}N$ device, although the breakdown voltage was observed to scale with Al composition. A critical electric field E_C = 8.1 MV/cm was extracted from the breakdown characteristic of the $Al_{0.57}Ga_{0.43}N$ device, although no correction was made to account for the very thin drift region, which analysis shows is severely punched-through. A dependence of critical electric field on bandgap of $E_C \sim E_G^{2.7}$ was derived from the experimental results, exceeding the prediction of Ref. [8]. Additionally, Xie et al. have reported Ni/Au Schottky diodes on $Al_xGa_{1-x}N$ with $x > 0.7$ [16]. These diodes, which had no field management structures, nevertheless showed breakdown voltage exceeding the theoretical limit of SiC. Finally, Hitchcock et al. demonstrated $Al_{0.8}Ga_{0.2}N$ Schottky diodes with $V_B > 5$ kV for a 5 µm thick n-drift layer doped at 5×10^{17} cm^{-3} [17]. These devices had no edge termination structures aside from a mesa etch. The Schottky diodes of both Refs. [16] and [17] were grown on insulating AlN substrates and thus had a quasi-vertical geometry with the cathode contact on the front surface of the wafer.

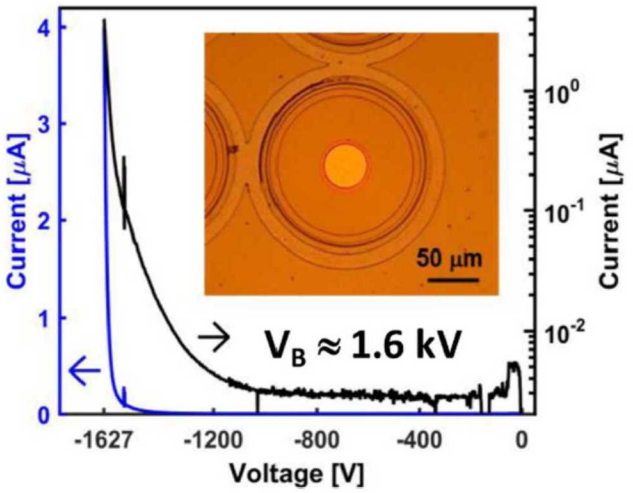

Fig. 5. Inset: Microscope image of quasi-vertical $Al_{0.7}Ga_{0.3}N$ pin diode. Main figure: Reverse IV characteristic of diode on linear (left) and logarithmic (right) scales. Reprinted from Ref. [18] with permission.

Work by our group at Sandia National Laboratories has focused on $Al_{0.3}Ga_{0.7}N$ pin diodes grown on AlN layers on thick

Sapphire substrates [18]. Due to the insulating substrate, these diodes had a quasi-vertical geometry. A Junction Termination Extension (JTE) field management structure was implemented using nitrogen implantation. The measured breakdown voltage exceeded 1.6 kV as shown in Fig. [5]. The breakdown voltage is somewhat soft, suggesting that mechanisms other than impact ionization may be contributing. Nevertheless, analyzing the breakdown (which is punch-through) yields an effective critical electric field of E_C = 5.9 MV/cm, consistent with the prediction of Ref. [8] for $Al_{0.3}Ga_{0.7}N$. The forward electrical characteristic is shown in Fig. 6, including a tangent line used to extract the differential specific on-resistance of $R_{on,sp}$ = 16 mΩ·cm^2. This is larger than what is expected from the UFOM for $Al_{0.3}Ga_{0.7}N$, which is likely due to the quasi-vertical geometry of the diode and the resulting lateral current flow that adds to the resistance of the device. Despite this, a high forward current density of 3.5 kA/cm^2 was achieved.

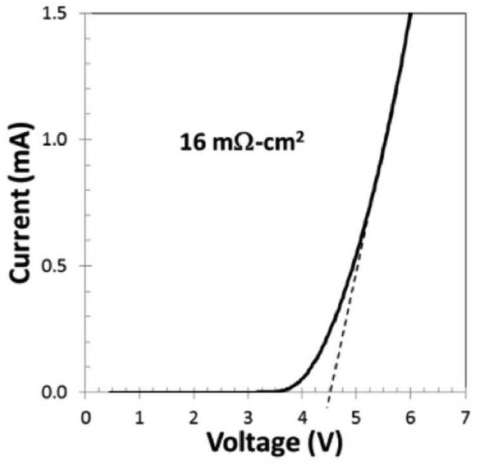

Fig. 6. Forward IV characteristic of quasi-vertical $Al_{0.3}Ga_{0.7}N$ pin diode, including tangent line used to extract differential on-resistance $R_{on,sp}$. Reprinted from Ref. [18] with permission.

III. Lateral AlGaN Power Switching Devices

A. Motivation

GaN-channel lateral power switching devices grown on Si substrates are continuing to grow in popularity – they are now offered commercially by multiple vendors and have been demonstrated in numerous power switching circuits [2]. It is therefore natural to ask whether the use of an $Al_yGa_{1-y}N/Al_xGa_{1-x}N$ heterostructure, or other lateral structures based on bulk or continuously-graded AlGaN alloys, have an advantage over conventional GaN-channel High Electron Mobility Transistors (HEMTs) based on the $Al_xGa_{1-x}N$/GaN with $x \sim 0.3$ or less. This question may be evaluated in a manner similar to that used for the vertical AlGaN devices discussed previously. It is found that a FOM equal to $V_B^2/R_{on,sp}$ is appropriate, as is true for the UFOM, but the theoretical expression for it is different. The relevant geometry is shown in Fig. 7, which is the lateral-device analogue to Fig. 2. In this case, the distance between the gate and the drain of the device is denoted by L, and the width of the device is W. A few differences are apparent compared to Fig. 2. First, the electric

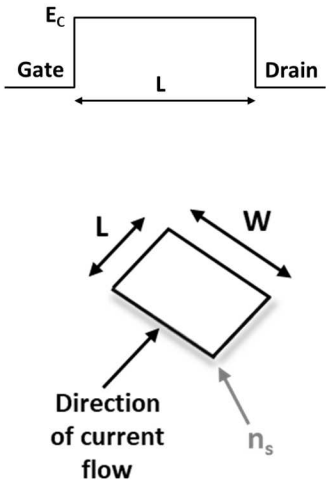

Fig. 7. Geometry relevant to derivation of the LFOM for lateral power switching devices.

field is not a linear function of position, but rather is constant as shown in the top portion of the figure. This is an idealized case, and in real devices the electric field tends to be peaked at the drain-side edge of the gate, necessitating the use of field plates and related structures [19,20]. The uniform field is the desired target, however, so it is used in the analysis. The critical value at which breakdown occurs, E_C, will be slightly different from the E_C discussed in the analysis of the vertical device, since the onset of avalanche breakdown occurs due to an integral (the ionization integral [7]) of the impact-ionization-generated carriers over the volume of the device, and does not simply occur when the electric field reaches a pre-determined value at a particular point within the device. Further, most lateral power devices do not actually exhibit avalanche breakdown, but rather breakdown due to effects at the surface, at an interface, etc. [1,2], so that an "effective" breakdown field, which is typically lower than the ideal breakdown field, must be used. Second, the direction of current flow, due to a 2D sheet density of carriers (n_s, measured in units of cm^{-2}) is parallel to the surface of the device as is shown in the bottom portion of Fig. 7, rather than perpendicular to it as is the case for the vertical device. By considering the breakdown voltage and the specific on-resistance dictated by the geometry of Fig. 7, an expression for the Lateral Figure-of-Merit, or LFOM, may be obtained:

$$LFOM = \frac{V_B^2}{R_{on,sp}} = q\mu_{ch} n_s E_C^2 \qquad (2)$$

The LFOM depends on the critical field squared, which is a weaker dependence than that for the UFOM. However, the sheet density n_s may be quite large in III-Nitride heterostructures, and in fact is expected to be larger in Al-rich heterostructures than in conventional AlGaN/GaN heterostructures due to the increase of the polarization coefficients with increasing Al composition [21]. The LFOM is compared to the UFOM for GaN-channel and $Al_{0.85}Ga_{0.15}N$-channel devices in Figure 8, assuming a sheet density of 10^{13} cm^{-2} for both cases (which likely underestimates n_s for the $Al_{0.85}Ga_{0.15}N$ case). It is seen that while the LFOM is superior to the UFOM for the GaN device, the opposite is true for the $Al_{0.85}Ga_{0.15}N$ device. Further, as noted in the inset of the figure and similar to the situation for the vertical device discussed previously, the mobility for AlGaN is dominated by alloy scattering, so the LFOM for an AlGaN-based device is expected to be insensitive to temperature, unlike the LFOM for a GaN-based device. While the analysis of the mobility in an Al-rich AlGaN heterostructure is slightly different than that for a vertical device – the mobility μ_{ch} appearing in Eq. (2) is the

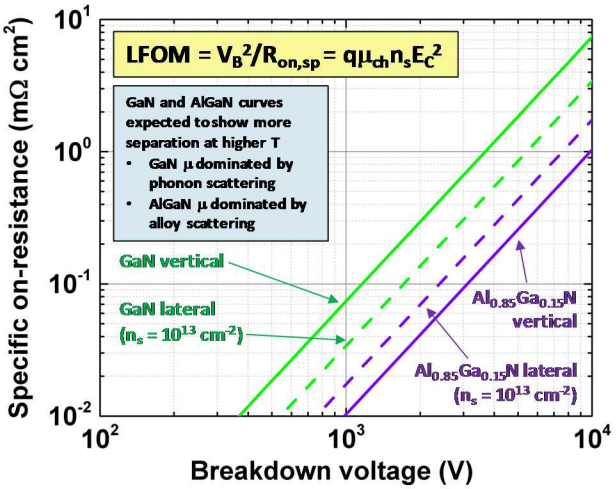

Fig. 8. UFOM and LFOM for GaN and $Al_{0.85}Ga_{0.15}N$ devices.

channel mobility, which may not equal the bulk mobility μ_n – the trends are the same, with a significant decrease in mobility occurring due to alloy scattering [22]. As such, like in the case for the vertical device, a trade-off exists between critical electric field and mobility, and a sufficiently high Al composition must be reached before improvements in performance relative to GaN can be expected.

B. Devices

The literature on lateral AlGaN power devices is considerably larger than that for vertical devices. As such, this section highlights some of the more significant results in this rapidly evolving field, and the reader is referred to the references for more detailed information. Several reports of AlGaN-channel HEMTs have been made by Nanjo et al. [23,24,25], including some of the earliest work circa 2008. These results were largely confined to lower Al compositions in $Al_yGa_{1-y}N/Al_xGa_{1-x}N$ heterostructures, with channel compositions $x < 0.4$ for these studies. Nevertheless, enhancement of breakdown voltage with increasing Al composition for equivalent device geometry was clearly demonstrated, and current densities of a few hundred mA/mm were shown, depending on the Al composition. Work by Tokuda and Yafune et al. [26,27] examined higher channel compositions in the 50-60% Al range. These devices achieved breakdown voltages in excess of 1.8 kV, but also showed lower saturation drain current density due to the difficulty in forming Ohmic contacts to the Al-rich barriers (up to pure AlN) used to achieve good carrier confinement. The difficulty in the formation of low-resistivity Ohmic contacts, and indeed in simply forming linear contacts to Al-rich AlGaN, is one of the major research challenges in the field today [28,29,30,31,32]. The work in Refs. [26] and [27] also showed the relative insensitivity of the drain current density to temperature, expected based on the dominance of alloy scattering in determining the mobility, as discussed in previous sections. Recent work by Muhtadi et al. [33] demonstrated a high drain current density of ~250 mA/mm for an $Al_{0.85}Ga_{0.15}N/Al_{0.65}Ga_{0.35}N$ heterostructure device, and Bajaj et al. [34] have utilized continuous compositional grading for Ohmic contact fabrication to achieve a drain current density of 500 mA/mm in a MOSFET structure consisting of an $Al_{0.7}Ga_{0.3}N$ channel and an Al_2O_3 dielectric.

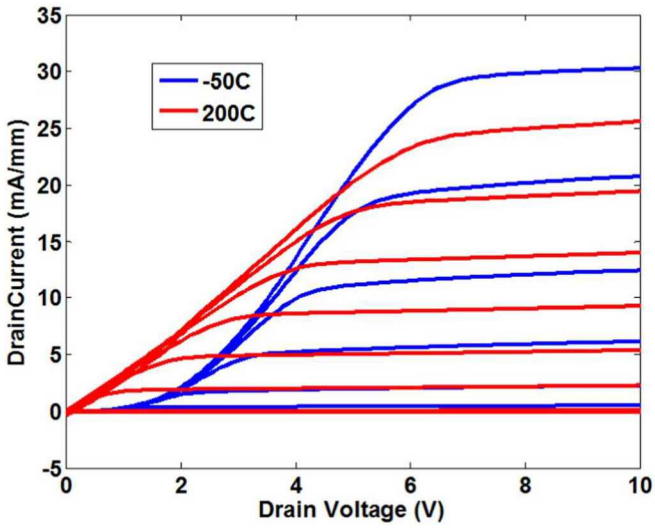

Fig. 9. I_D-V_{DS} curves for $Al_{0.85}Ga_{0.15}N/Al_{0.70}Ga_{0.30}N$ Schottky-gated HEMT measured at -50 and 200°C. Gate voltage ranges from -3 to +2 V with a step of 1 V. Reprinted from Ref. [36] with permission.

Our group at Sandia has worked on various aspects of Al-rich AlGaN transistors. Our first reported device results were based on

an AlN/$Al_{0.85}Ga_{0.15}N$ heterostructure [35], which showed good breakdown voltage, although the current density was limited by the Ohmic contacts. Subsequent work has focused on the development of Ohmic contacts [31,32] and HEMTs with improved current density and robustness over a wide temperature range based on an $Al_{0.85}Ga_{0.15}N/Al_{0.70}Ga_{0.30}N$ heterostructure [36]. The I_D-V_{DS} curves for this Schottky-gated device, measured at -50 and 200°C, are shown in Fig. 9. Reasonable saturation current density is seen at both temperature extremes, and improvement in the Ohmic contacts is observed at high temperature (this is especially evident in the removal of the voltage offset that is apparent at the lower temperature). The transfer characteristics for the same device are shown in Fig. 10 and demonstrate the robustness of the device over a wide temperature range. An Arrhenius plot of the leakage current is shown in the inset, from which an activation energy of 0.55 eV is obtained. Breakdown measurements on similar devices yielded an effective critical electric field of 250 V/μm. Other recent work by our group has focused on additional high-temperature AlGaN device measurements [37,38], normally-on operation [39,40], polarization-doped FETs (PolFETs) [41,42], reliability [43], and radiation effects [44].

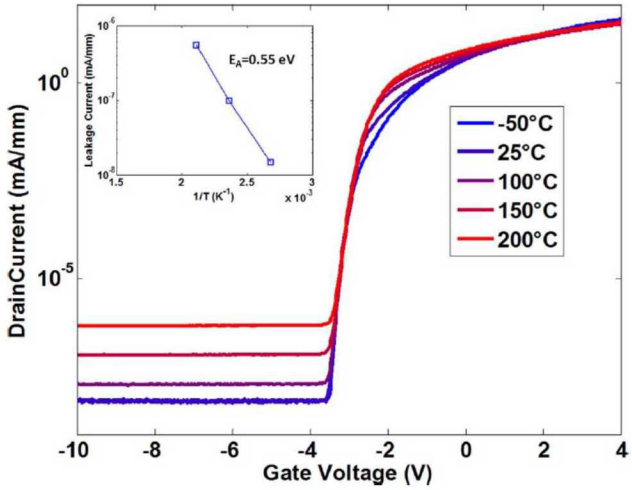

Fig. 10. Main figure: Transfer curves for $Al_{0.85}Ga_{0.15}N/Al_{0.70}Ga_{0.30}N$ Schottky-gated HEMT measured at various temperatures. Inset: Arrhenius plot of leakage current. Reprinted from Ref. [36] with permission.

IV. Lateral AlGaN Radio-Frequency Devices

A. Motivation

The relevant figure-of-merit for an RF device is the Johnson FOM (JFOM) which considers the breakdown voltage V_B and the frequency f_T at which unity current gain occurs [45]:

$$JFOM = V_B f_T = \frac{E_C v_{sat}}{2\pi} \quad (3)$$

The JFOM may be derived by considering the breakdown voltage under a constant-field scenario (similar to the top portion of Fig. 7), the gate capacitance and resulting gate current, and the transit time of carriers (electrons) beneath the gate. Because RF devices are designed such that the electric field in the gate region is high, the velocity of the electrons is saturated, i.e. it is not proportional to electric field, as is the case for power switching devices (the mobility is the proportionality constant between electron velocity and electric field at low fields). Thus, the relevant transport

property is the saturation velocity v_{sat}, rather than the low-field mobility. Monte-Carlo calculations of the saturation velocity for several compositions x of $Al_xGa_{1-x}N$ indicate that v_{sat} is relatively insensitive to alloy composition [46]. That is, while the saturation velocity shows a slight dip for alloyed material, it is nowhere near as pronounced as the dip is for the low-field mobility. A recent study has reported $v_s = 3.8\times10^6$ cm/s for $Al_{0.70}Ga_{0.30}N$ [47], somewhat below the value predicted in Ref. [46]. By interpolating across the discrete Al compositions evaluated in Ref. [46] and combining this with the E_C prediction shown in Fig. 1, a plot of the expected JFOM as function of Al composition may be obtained and is shown in Fig. 11. While the dip in v_{sat} for intermediate compositions is small, the JFOM only depends linearly on E_C, so a small dip in the JFOM is observed for lower Al compositions. Nevertheless, for Al compositions above about 40% an increase in the predicted JFOM is observed, which for Al-rich AlGaN reaches a factor of ~4 relative to GaN.

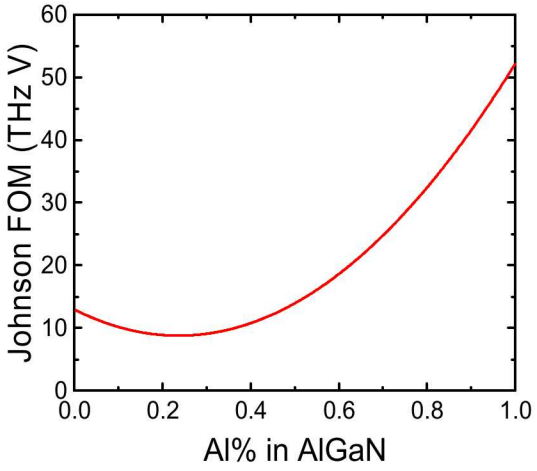

Fig. 11. Calculation of expected JFOM as a function of Al% for AlGaN alloys.

B. Devices

Several theoretical and experimental studies on AlGaN RF transistors have been published. Sohel et al. [48] demonstrated X-band operation of PolFETs utilizing a compositionally-graded $Al_xGa_{1-x}N$ channel, with x varying from 0 to 0.4 over a distance of 20 nm. This device achieved peak f_T and f_{max} of 23 and 65 GHz respectively for a device with a gate length of 0.7 μm and a width of 2×75 μm. The peak power of this device was 2 W/mm. The same group also reported an RF device based on an $Al_{0.75}Ga_{0.25}N/Al_{0.60}Ga_{0.40}N$ heterostructure, coupled with compositional grading for the Ohmic contacts, with $f_T = 40$ GHz and $f_{max} = 58$ GHz [49].

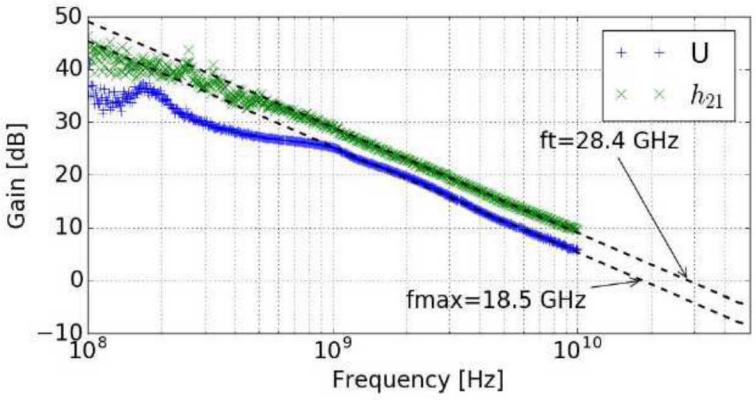

Fig. 12. Small-signal RF measurements of $Al_{0.85}Ga_{0.70}N/Al_{0.70}Ga_{0.30}N$ HEMT with 80 nm gate length at $V_{GS} = 2.75$ V, $V_{DS} = 20$ V. Reprinted from Ref. [51] with permission.

Our group at Sandia has conducted simulations to examine the potential

performance of RF HEMTs based on $Al_yGa_{1-y}N/Al_xGa_{1-x}N$ heterostructures [50]. A device consisting of an AlN barrier, an $Al_{0.70}Ga_{0.30}N$ channel, and an $Al_{0.78}Ga_{0.22}N$ back-barrier was simulated using TCAD. Small-signal simulations indicated that f_T = 46 GHz, f_{max} = 230 GHz, and a gain of 34 dB at 30 GHz are achievable for this design. Further, load-pull simulations yielded a saturated power density of 18 W/mm, a Power-Added Efficiency (PAE) of 55%, and a third-order intercept point > 40 dBm. Our group has also fabricated and tested RF transistors based on an $Al_{0.85}Ga_{0.15}N/Al_{0.70}Ga_{0.30}N$ heterostructure [51]. All devices had a gate length of 80 nm. Small-signal RF measurements were performed on a device with source-gate spacing of 0.5 µm, gate-drain spacing of 2.0 µm, and gate width of 2×50 µm at V_{GS} = 2.75V, V_{DS} = 20 V. The results of this measurement are shown in Fig. 12. The measurements yielded f_T = 28.4 GHz and f_{max} = 18.5 GHz. The reversal in frequency order of f_T and f_{max} from what is expected may be due to gate resistance and/or drain conductance. Large-signal load-pull measurements at 3 GHz with the device biased at V_{GS} = 3.75 V, V_{DS} = 20 V to approximate class-A operation are shown in Fig. 13. The output power at maximum PAE (11%) was P_{OUT} = 0.38 W/mm, or equivalently 15.8 dBm. Maximum power gain and transducer gain were G_P = 5.8 dB and G_T = 7.3 dB, respectively. While these results fall below the simulated predictions (which may be due to limitations of the Ohmic contacts), they nevertheless show the potential of Al-rich AlGaN for RF applications.

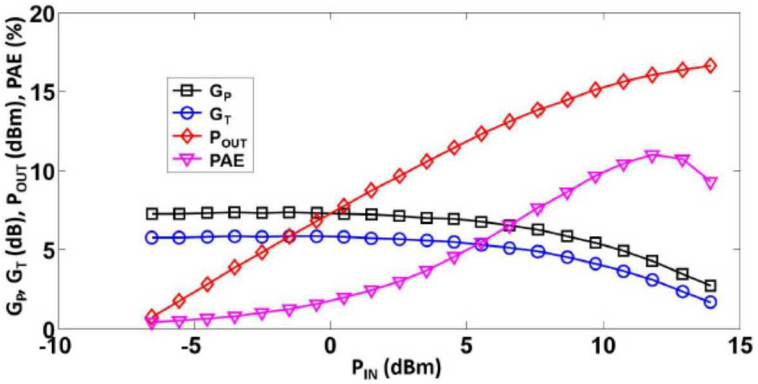

Fig. 13. Large-signal RF measurements of $Al_{0.85}Ga_{0.70}N/Al_{0.70}Ga_{0.30}N$ HEMT with 80 nm gate length at V_{GS} = 3.75 V, V_{DS} = 20 V. Reprinted from Ref. [51] with permission.

V. Conclusion

This chapter has reviewed the properties of UWBG AlGaN that make it a potential candidate for next-generation power switching and radio-frequency devices. It has been shown that the increase of the critical electric field with increasing bandgap drives improvements in the figures of merit relevant to power switching devices (UFOM and LFOM for vertical and lateral geometries, respectively) and RF devices (JFOM for lateral geometries). Further, examples of published device results from our group and other groups have been reviewed. Highlights include a measured effective critical electric field of 5.9 MV/cm for a vertical $Al_{0.30}Ga_{0.70}N$ pin diode, robust operation of an $Al_{0.85}Ga_{0.15}N/Al_{0.70}Ga_{0.30}N$ power switching HEMT over a temperature range of -50°C to 200°C, and an output power of 3.8 W/mm at 3 GHz for an RF HEMT. These experimental results demonstrate that UWBG AlGaN is indeed viable for demanding future power and RF applications. The field is presently expanding significantly and is examining different device designs as well as

processing challenges. One of the foremost among these challenges is the formation of low-resistivity Ohmic contacts to Al-rich AlGaN. Rapid progress is being made in resolving this and other challenges, suggesting that the future is very promising for UWBG AlGaN.

Acknowledgement

This work was partially supported by the Laboratory-Directed Research and Development program at Sandia National Laboratories, a multi-mission laboratory managed and operated by National Technology & Engineering Solutions of Sandia, LLC, a wholly owned subsidiary of Honeywell International Inc., for the U.S. Department of Energy's National Nuclear Security Administration under contract DE-NA0003525. The views expressed in this article do not necessarily represent the views of the U.S. Department of Energy or the United States Government.

References

1. M. Meneghini, G. Meneghesso, and E. Zanoni, Eds., *Power GaN Devices*, Springer (2017).
2. H. Amano et al., "The 2018 GaN Power Electronics Roadmap," *J. Phys. D.* **51**, 163001 (2018).
3. R. Quay, *Gallium Nitride Electronics*, Springer (2008).
4. R. S. Pengelly, S. M. Wood, J. W. Milligan, S. T. Sheppard, and W. L Pribble, "A Review of GaN-on-SiC High Electron Mobility Transistors and MMICs," *IEEE Trans. Microwave Theory Tech.* **60(6)**, 1764 (2012).
5. J. Y Tsao et al., "Ultrawide-Bandgap Semiconductors: Research Opportunities and Challenges," *Adv. Elec. Mat.* **4**, 1600501 (2018).
6. R. J. Kaplar, J. C. Neely, D. L. Huber, and L. J. Rashkin, "Generation-After-Next Power Electronics," *IEEE Power Elec. Mag.* **4 (1)**, 36 (2017).
7. B. J. Baliga, *Fundamentals of Power Semiconductor Devices,* Springer (2008).
8. J. L. Hudgins, G. S. Simin, E. Santi, and M. A. Khan, *IEEE Trans. Power Elec.* **18(3)**, 907 (2003).
9. Y. H. Liang and E. Towe, "Progress in Efficient Doping of High Aluminum-Containing Group-III Nitrides," *Appl. Phys. Rev.* **5**, 011107 (2018).
10. J. Simon, V. Protasenko, C. Lian, H. Xing, and D. Jena, "Polarization-Induced Hole Doping in Wide-Bandgap Uniaxial Semiconductor Heterostructures," *Science* **327**, 60 (2010).
11. R. J. Kaplar, A. A. Allerman, A. M. Armstrong, M. H. Crawford, J. R. Dickerson, A. J. Fischer, and E. A. Douglas, "Review – Ultra-Wide-Bandgap AlGaN Power Electronic Devices," *ECS J. Solid State Sci. Tech.* **6(2)**, Q3061 (2017).
12. M. E. Coltrin and R. J. Kaplar, "Transport and Breakdown Analysis for Improved Figure-of-Merit for AlGaN Power Devices," *J. Appl. Phys.* **121**, 055706 (2017).
13. S. Bajaj, T. H. Hung, F. Akyol, D. Nath, and S. Rajan, "Modeling of High Composition AlGaN-Channel HEMTs with Large Threshold Voltage," *Appl. Phys. Lett.* **105**, 263503 (2014).
14. A. Nishikawa, K. Kumakura, T. Akasaki, and T. Makimoto, "High Critical Electric Field of $Al_xGa_{1-x}N$ p-i-n Vertical Conducting Diodes on n-SiC Substrates," *Appl. Phys. Lett.* **88**, 173508 (2006).
15. A. Nishikawa, K. Kumakura, and T. Makimoto, "High Critical Electric Field Exceeding 8 MV/cm Measured Using an AlGaN p-i-n Vertical Conducting Diode on n-SiC Substrate," *Jpn. J. Appl. Phys.* **46(4B),** 2316 (2007).

16. J. Xie, S. Mia, R. Dalmau, R. Collazo, A. Rice, J. Tweedie, and Z. Sitar, "Ni/Au Schottky Diodes on $Al_xGa_{1-x}N$ Grown on AlN Single Crystal Substrates," *Phys. Stat. Sol*. **8(7-8)**, 2407 (20111).
17. C. Hitchcock, G. Panday, T. P. Chow, B. Moody, S. Mita, J. Smart, and R. Dalmau, "First Experimental Demonstration of High-Voltage, Quasi-Vertical Al0.8Ga0.2N Schottky Diodes on AlN Substrates," *Int. Conf. Nit. Semi.* (ICNS), Strasbough, France (2017).
18. A. A. Allerman, A. M. Armstrong, A. J. Fischer, J. R. Dickerson, M. H. Crawford, M. P. King, M. W. Moseley, J. J. Wierer, and R. J. Kaplar, "$Al_{0.3}Ga_{0.7}N$ PN Diode with Breakdown Voltage > 1600 V," *Elec. Lett.* **52(15)**, 1319 (2016).
19. H. Xing, Y. Dora, A. Chini, S. Heikman, S. Keller, and U. K. Mishra, "High Breakdown Voltage AlGaN-GaN HEMTs Achieved by Multiple Field Plates," *IEEE Elec. Dev. Lett.* **25(4)**, 161 (2004).
20. B. D. Tierney, S. Choi, S. DasGupta, J. R. Dickerson, S. Reza, R. J. Kaplar, A. G. Baca, and M. J. Marinella, "Evaluation of a 'Field Cage' for Electric Field Control in GaN-Based HEMTs that Extends the Scalability of Breakdown into the kV Regime," *IEEE Trans Elec. Dev.* **64(9)**, 3740 (2017).
21. F. Bernardini V. Fiorentini, and D. Vanderbilt, "Spontaneous Polarization and Piezoelectric Constants of III-N Materials," *Phys. Rev. B* **56(16)**, R10024 (1997).
22. M. E. Coltrin, A. G. Baca, and R. J. Kaplar, "Analysis of 2D Transport and Performance Characteristics for Lateral Power Devices Based on AlGaN Alloys", *ECS J. Solid State Sci. Tech.* **6**, S3114 (2017).
23. T. Nanjo, M. Takeuchi, M. Suita, Y. Abe, T. Oishi, Y. Tokuda, and Y. Aoyagi, "First Operation of AlGaN-Channel High Electron Mobility Transistors," *Appl. Phys. Exp.* **1**, 011101 (2008).
24. T. Nanjo, M. Takeuchi, M. Suita, T. Oishi, Y. Abe, Y. Tokuda and Y. Aoyagi, "Remarkable Breakdown Voltage Enhancement in AlGaN-Channel High Electron Mobility Transistors," *Appl. Phys. Lett.* **92**, 263502 (2008).
25. T. Nanjo, A. Imai, Y. Suzuki, Y. Abe, T. Oishi, M. Suita, E. Yagyu, and Y. Yasunori," AlGaN Channel HEMT with Extremely High Breakdown Voltage," *IEEE Trans. Elec. Dev.* **60(3)**, 1046 (2013).
26. H. Tokuda, M. Hatano, N. Yafune, S. Hashimoto, K. Akita, Y. Yamamoto, and M. Kuzuhara, "High Al Composition AlGaN-Channel High Electron Mobility Transistor on AlN Substrate," *Appl. Phys. Exp.* **3**, 121003 (2010).
27. N. Yafune, S. Hashimoto, K. Akita, Y. Yamamoto, H. Tokuda, and M. Kuzuhara, "AlN/AlGaN HEMTs on AlN Substrate for Stable High-Temperature Operation," *Elec. Lett.* **50(3)**, 211 (2014).
28. N. Yafune, S. Hashimoto, K. Akita, Y. Yamamoto and Kuzuhara, "Low-Resistive Ohmic Contacts for AlGaN-Channel High Electron Mobility Transistors Using Zr/Al/Mo/Au Metal Stack," *Jpn. J. Appl. Phys.* **50**, 100202 (2011).
29. P. S. Park, S. Krishnamoorthy, S. Bajaj, D. N. Nath, and S. Rajan, "Recess-Free Non-Alloyed Ohmic Contacts on Graded AlGaN Heterojunction FETs," *IEEE Elec. Dev. Lett.* **36(3)**, 226 (2015).
30. S. Bajaj, F. Akyol, S. Krishnamoorthy, Y. Zhang, and S. Rajan, "AlGaN-Channel Field Effect Transistors with Graded Heterostructure Ohmic Contacts," *Appl. Phys. Lett.* **109**, 133508 (2016).
31. E. A. Douglas, S. Reza, C. Sanchez, D. Koleske, A. Allerman, B. Klein, A. M. Armstrong, R. J. Kaplar, and A. G. Baca, "Ohmic Contacts to Al-rich AlGaN Heterostructures," *Phys. Stat. Sol. A* **214**, 1600842 (2017).
32. B. A. Klein, A. G. Baca, A. M. Armstrong, A. A. Allerman, C. A. Sanchez, E. A. Douglas, M. H. Crawford, M. A. Miller, P. G. Kotula, T. R. Fortune, and V. M. Abate, "Planar Ohmic Contacts to $Al_{0.45}Ga_{0.55}N/Al_{0.30}Ga_{0.70}N$ High Electron Mobility Transistors," *ECS J. Solid State Sci. Tech.* **6**, S3067 (2017).

33. S. Muhtadi, S. M. Hwang, A. Coleman, F. Asif, G. Simin, M. V. S. Chandrashekhar, and A. Khan, "High Electron Mobility Transistors with $Al_{0.65}Ga_{0.35}N$ Channel Layers on Thick AlN/Sapphire Templates," *IEEE Elec. Dev. Lett.* **38(7)**, 914 (2017).
34. S. Bajaj, A. Allerman, A. Armstrong, T. Razzak, V. Talesara, W. Sun, S. Sohel, Y. Zhang, W. Lu, A. R. Arehart, F. Akyol, and S. Rajan, "High Al-Content AlGaN Transistor with 0.5 A/mm Current Density and Lateral Breakdown Field Exceeding 3.6 MV/cm," *IEEE Elec. Dev. Lett.* **39(2)**, 256 (2018).
35. A. G. Baca, A. M. Armstrong, A. A. Allerman, E. A. Douglas, C. A. Sanchez, M. P. King, M. E. Coltrin, T. R. Fortune, and R. J. Kaplar, "An $AlN/Al_{0.85}Ga_{0.15}N$ High Electron Mobility Transistor,**"** *Appl. Phys. Lett.* **109**, 033509 (2016).
36. A. G. Baca , B. A. Klein, A. A. Allerman, A. M. Armstrong, E. A. Douglas, C. A. Stephenson, T. R. Fortune, and R. J. Kaplar, "$Al_{0.85}Ga_{0.15}N/Al_{0.70}Ga_{0.30}N$ High Electron Mobility Transistors with Schottky Gates and Large On/Off Current Ratio over Temperature," *ECS J. Solid State Sci. Tech.* **6(12)**, Q161 (2017).
37. A. G. Baca, A. M. Armstrong, A. A. Allerman, B. A. Klein, E. A. Douglas, C. A. Sanchez, and T. R. Fortune, "High-Temperature Operation of $Al_{0.45}Ga_{0.55}N/Al_{0.30}Ga_{0.70}N$ High Electron Mobility Transistors," *ECS J. Solid State Sci. Tech.*, **6(11)**, S3010 (2017).
38. P. H. Carey IV, F. Ren, A. G. Baca, B. A. Klein, A. A. Allerman, A. M. Armstrong, E. A. Douglas, R. J. Kaplar, P. G. Kotula, and S. J. Pearton, "Operation up to 500°C of $Al_{0.85}Ga_{0.15}N/Al_{0.70}Ga_{0.30}N$ High Electron Mobility Transistors," *IEEE J. Elec. Dev. Soc.* **7**, 444 (2019).
39. E. A. Douglas, B. Klein, A. A. Allerman, A. G. Baca, T. Fortune, and A. M. Armstrong, "Enhancement-Mode AlGaN-Channel High Electron Mobility Transistor Enabled by p-AlGaN Gate," *J. Vac. Sci. Tech B* **37**, 021208 (2019).
40. B. A. Klein, E. A. Douglas, A. M. Armstrong, A. A. Allerman, V. M. Abate, T. R. Fortune, and A. G. Baca, "Enhancement-Mode $Al_{0.85}Ga_{0.15}N/Al_{0.70}Ga_{0.30}N$ High Electron Mobility Transistor with Fluorine Treatment," *Appl. Phys. Lett.* **114**, 112104 (2019).
41. A. M. Armstrong, B. A. Klein, A. Colon, A. A. Allerman, E. A. Douglas, A. G. Baca, T. R. Fortune, V. M. Abate, S. Bajaj, and S. Rajan, "Ultra-Wide-Bandgap AlGaN Polarization-Doped Field-Effect Transistor," *Jpn. J. Appl. Phys.* **57**, 074103 (2018).
42. A. M. Armstrong, B. A. Klein, A. G. Baca, A. A. Allerman, E. A. Douglas, A. Colon, V. M. Abate, and T. R. Fortune "AlGaN Polarization-Doped Field-Effect Transistor with Compositionally-Graded Channel from $Al_{0.6}Ga_{0.4}N$ to AlN," *Appl. Phys. Lett.* **114**, 052103 (2019).
43. A. G. Baca, B. A. Klein, A. M. Armstrong, A. A. Allerman, E. A. Douglas, T. R. Fortune, and R. J. Kaplar, "Stability in Fluorine-Treated Al-Rich High Electron Mobility Transistors with 85% Barrier Composition", *IEEE Int. Rel. Phys. Symp.,* Monterey, CA (2019).
44. M. J. Martinez, M. P. King, A. G. Baca, A. A. Allerman, A. A. Armstrong, B. A. Klein, E. A. Douglas, R. J. Kaplar, and S. E. Swanson, "Radiation Response of AlGaN-Channel HEMTs," *IEEE Trans. Nuc. Sci.* **66(1)** 344 (2019).
45. E. Johnson, "Physical Limitations on Frequency and Power Parameters of Transistors," *RCA Rev.* **26**, 163 (1965).
46. E. Bellotti and F. Bertazzi, "A Numerical Study of Carrier Impact Ionization AlGaN," *J. Appl. Phys.* **111**, 103711 (2012).
47. B. A. Klein, A. G. Baca, S. M. Lepkowski, C. D. Nordquist, J. R. Wendt, A. A. Allerman, A. M. Armstrong, E. A. Douglas, V. M. Abate, and R. J. Kaplar, "Saturation Velocity Measurement of

$Al_{0.7}Ga_{0.3}N$-Channel High Electron Mobility Transistors," *J. Elec. Mat.* DOI 10.1007/s11664-019-07421-1 (2019).
48. S. H. Sohel, A. Xie, E. Beam, H. Xue, J. A. Roussos, T. Razzak, S. Bajaj, Y. Cao, D. J. Meyer, W. Lu, and S. Rajan, "X-Band Power and Linearity Performance of Compositionally-Graded AlGaN Channel Transistors," *IEEE Elec. Dev. Lett.* **39(12)**, 1884 (2018).
49. H. Xue, C. H. Lee, K. Hussian, T. Razzak, M. Abdullah, Z. Xia, S. H. Sohel, A. Khan, S. Rajan, and W. Lu, "$Al_{0.75}Ga_{0.25}N/Al_{0.60}Ga_{0.40}N$ Heterojunction Field-Effect Transistor with f_T of 40 GHz," *Appl. Phys. Exp.* **12**, 066502 (2019).
50. S. Reza, B. A. Klein, A. G. Baca, A. M. Armstrong, A. A. Allerman, E. A. Douglas, and R. J. Kaplar, "High-Frequency, High-Power Performance of AlGaN-Channel High Electron Mobility Transistors: An RF Simulation Study," *Jpn. J. Appl. Phys.* **58**, SCCD04 (2019).
51. A. G. Baca, B. A. Klein, J. R. Wendt, S. M. Lepkowski, C. D. Nordquist, A. M. Armstrong, A. A. Allerman, E. A. Douglas, and R. J. Kaplar, "RF Performance of AlGaN-Channel $Al_{0.85}Ga_{0.15}N/Al_{0.70}Ga_{0.30}N$ High Electron Mobility Transistors with 80 nm Gates," *IEEE Elec. Dev. Lett.* **40(1)**, 17 (2019).